Molecular Dynamics Simulation of Diffusion in Pillared Clays

Xiaohua Yi and Katherine S. Shing
Dept. of Chemical Engineering, University of Southern California, Los Angeles, CA 90089

Muhammad Sahimi
Dept. of Chemical Engineering, University of Southern California, Los Angeles, CA 90089
HLRZ Supercomputer Center, KFA Jülich, 52425 Jülich, Germany

The thermodynamics and transport properties of Lennard-Jones particles in pillared catalytic clays are studied by molecular dynamics simulation. The clays are represented by parallel sheets separated by a given distance and connected by pillars of a given size. Two different spatial distributions of the pillars are studied to determine their effect on the properties of the system. Calculations did not indicate a strong dependence of the diffusivity on the spatial distribution of the pillars, except at low porosities. The solvation force increases monotonically with decreasing porosity of the clays and increasing density of the molecules. The percolation threshold φ_c of the system is estimated from the diffusivity measurements in the limit of infinitely low sorbate densities. Near φ_c the diffusivity D vanishes according to the power law, $D \sim (\varphi - \varphi_c)^n$, where φ is the porosity of the system, and n is a universal constant. The simulations yield $n \simeq 1.7$. Since 2-D percolation systems require $n \simeq 1.3$ and 3-D systems $n \simeq 2.0$, pillared clays behave as a system with an effective dimensionality between 2 and 3.

Introduction

Diffusion and reaction in porous catalysts have been the subject of considerable research activity in the last few years (for a review see Sahimi et al., 1990). These systems, in addition to their great industrial importance, also represent ideal model porous systems well-suited for theoretical and experimental studies of hindered diffusion, adsorption, and reaction phenomena (for reviews and references see Deen, 1987; Sahimi, 1992). Such phenomena, which involve the transport and reaction of large molecules in small pores, occur also in many processes of current scientific and industrial interest, such as separation processes, solvent swelling rubbers, polyelectrolyte gels, enzyme immobilization in porous solids, and size exclusion chromatography. Numerous experimental and theoretical studies have found hindered transport and reaction processes in porous media to be less efficient than unhindered transport in an unbounded solution. This reduced efficiency is generally caused by the molecules' being excluded from a fraction of the pore volume, and by the hydrodynamics resistance hindering the transport of the molecules through the porous medium.

Among all catalytic systems, which are of prime interest in this article, zeolites have received the greatest attention (Kerr, 1989). But considerable less attention and research effort have been focused on studying diffusion and reaction phenomena in another class of catalytic materials, namely, pillared clays (for reviews see Pinnavaia, 1983; Laszlo, 1987), although there have recently been several studies of such systems, most of which are experimental in nature (see, for example, Occelli et al., 1985; Lee et al., 1989). The original idea for producing pillared clays, due to Barrer and MacLeod (1955), was to insert molecules into clay minerals to prop apart the aluminosilicate sheets, thereby producing larger pores than in native clays, or even in zeolites. However, such materials did not have the thermal stability that zeolites usually possess. But pillars of hydroxyaluminum and other cations, which are capable of being dehydrated to oxide pillars and to support temperatures of up to 500°C without structural collapse under catalytic cracking conditions, are relatively new and were first reported by Brindley and Sempels (1977) and independently by Lahav et al. (1978) and Vaughan and Lussier (1980).

In general, pillared montmorillomites are 2:1 dioctahedral

Correspondence concerning this article should be addressed to M. Sahimi.

clay minerals consisting of layers of silica in tetrahedral coordination, holding between them a layer of alumina in octahedral coordination. Substituting Si^{4+} with Al^{3+}, or Al^{3+} with Mg^{2+}, gives the silicate layer a negative net charge, which is normally compensated by Na^{+}, Ca^{2+}, and Mg^{2+} ions (Grim, 1986). By exchanging the charge-compensating cations with large cationic oxyaluminum polymers, one can synthesize molecular sieve-type materials (Lahav et al., 1978; Vaughan and Lussier, 1978). These inorganic polymers, when heated, form pillars that prop open the clay layer structure and form permanent pillared clays.

The restricted structure of pillared clays has prompted some researchers to suggest that they behave as systems with an effective dimensionality less than three, since molecules are forced to move in a very restricted pore space between the silicate layers. However, such a suggestion has not yet been quantified. The molecules might also be able to move from one layer to another, although this may be difficult, especially if the molecular sizes are large. There have been some speculations (van Damme and Fripiat, 1985) that pillared clays may have a fractal structure, both in terms of the surface of the pillars and the volume of the pore space. If this is the case, it can have important implications for diffusion and reaction in pillared clays, since the behavior of such phenomena in fractal systems cannot be described by the classical equations of transport and reaction.

Pillared clays have shown high catalytic activities for gas oil cracking, similar to zeolite-based catalysts. They have also shown large initial activities toward methanol conversion to olefins and toluene ethylation, but they are substantially deactivated by coke deposition (Figueras, 1988). One reason for the interest in pillared clays is that their pore sizes can be made larger than those of faujastic zeolites. Moreover, since access to the interior pore volume of pillared clays is controlled by the distance between the silicate layers and also the distance between the pillars, one or both distances may be adjusted to suit a particular application. It has also been suggested that they are a new class of sorbents for gas separations (Yang and Baksh, 1991).

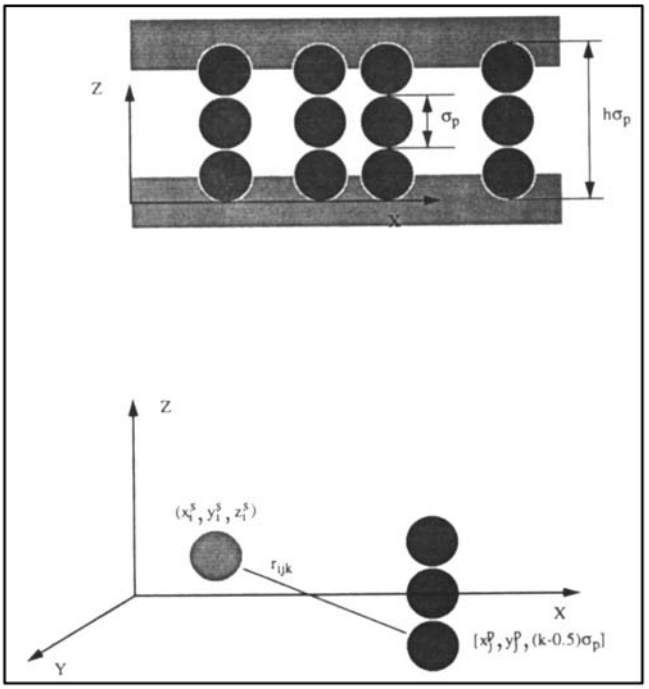

Figure 1. Pillared clays and calculations of the distance between a sorbate particle and a pillar unit.

Despite their industrial importance and the wealth of experimental information currently available, and in spite of the fact that pillared clays can provide a testing ground for various theories of transport and reaction in catalytic systems and other porous media, no fundamental theoretical effort has been undertaken so far to investigate transport and reaction processes in pillared clays. To the best of our knowledge, there have been only two computer simulation studies of pillared clays. Sahimi (1990) used a model of the clays, somewhat similar to that employed here, together with rodlike molecules and simple random walk simulations to gain qualitative insight into diffusion in pillared clays. Cracknell et al. (1993) studied the adsorption isotherms and the heat of adsorption of inert gases in the pillared clays by using grand canonical ensemble Monte Carlo (GCEMC) simulation. In this article we use molecular dynamics simulations to study diffusion of finite-size molecules in model pillared clays.

The plan of this article is as follows. In the next section we describe the model of pillared clays that we use. Next we discuss the details of our computational procedures. We then present our results and discuss their implications. The article is summarized in the last section.

Model Representation

To study diffusion in pillared clays, we first develop a model to represent the clays, which is shown schematically in Figure 1. The surface of the solid walls are assumed to be the (100) face of a face-centered cubic (FCC) solid. The pillars, which consist of a given number of atoms or groups, are assumed to be distributed either randomly or uniformly between the solid walls. Two parameters, the separation between the solid walls h and the porosity of the system φ are used to characterize the morphology of the clays. The separation h is defined as the distance between the center of the atoms on the surface layers of the upper and lower solid walls. The nominal porosity φ of the system is given by (see Figure 1)

$$\varphi = 1 - \frac{N_p \pi \sigma_p^2}{6l^2}, \tag{1}$$

where N_p is the number of pillars inside a $l \times l \times (h-1)\sigma_p$ cell, and σ_p is the characteristic diameter of the pillar components.

The following potential function

$$\phi(r) = \begin{cases} \phi_{LJ}(r) - \phi_{LJ}(r_c) & \text{if } r \le r_c \\ 0 & \text{if } r > r_c \end{cases} \tag{2}$$

is used to describe the interactions between sorbate particles as well as between sorbate particles and the pillars, where r_c

is the truncation distance of the potential. Here ϕ_{LJ} is the Lennard-Jones potential

$$\phi_{LJ}(r) = 4\epsilon\left[\left(\frac{\sigma}{r}\right)^{12} - \left(\frac{\sigma}{r}\right)^{6}\right], \tag{3}$$

where ϵ and σ are the usual energy and size parameters, respectively. The advantage of using this form of the potential is that it avoids the long-range corrections, which are difficult to evaluate accurately for our system due to the presence of the solid walls (Snook and van Megan, 1980). Assuming pairwise additivity and a rigid solid, the instantaneous potential energy between all sorbate particles and the pillars can be written as

$$\psi_{sp} = 4\epsilon_{sp}\sum_{i=1}^{N_s}\sum_{j=1}^{N_p}\sum_{k=1}^{h}\left[\left(\frac{\sigma_{sp}}{r_{ijk}}\right)^{12} - \left(\frac{\sigma_{sp}}{r_{ijk}}\right)^{6}\right], \tag{4}$$

where N_s is the numbers of sorbate particles, ϵ_{sp} and σ_{sp} are the parameters associated with the pillar-sorbate interaction, and r_{ijk} is the distance between the ith sorbate particle and the kth unit of the jth pillar (see Figure 1), which is given by

$$r_{ijk}^2 = (x_i^s - x_j^s)^2 + (y_i^s - y_j^s)^2 + [z_i^s - (k-0.5)\sigma_p]^2, \tag{5}$$

where x_i^s, y_i^s, and z_i^s are the coordinates of the ith sorbate particle. Similarly, the instantaneous potential energy associated with the sorbate-sorbate interactions is given by

$$\psi_{ss} = 4\epsilon_{ss}\sum_{i=1}^{N_s}\sum_{j<i}^{N_s}\left[\left(\frac{\sigma_{ss}}{r_{ij}}\right)^{12} - \left(\frac{\sigma_{ss}}{r_{ij}}\right)^{6}\right], \tag{6}$$

where r_{ij} is the distance between sorbate pair i and j, and ϵ_{ss} and σ_{ss} are the parameters describing sorbate-sorbate interaction. The potential function employed to describe the interaction between sorbate particles and the solid walls is the one suggested by Steele (1973)

$$\psi_{sw} = 2\pi\epsilon_{sw}\sum_{i=1}^{N_s}\left[\frac{2}{5}\left(\frac{\sigma_{sw}}{z_i}\right)^{10} - \left(\frac{\sigma_{sw}}{z_i}\right)^{4} - \frac{0.4714}{(z_i/\sigma_{sw}+0.4314)^3}\right], \tag{7}$$

which is the result of a mean-field approximation of the interaction between a sorbate particle and a Lennard-Jones-type FCC solid with surface density 1.0. Here ϵ_{sw} and σ_{sw} are parameters used in the potential for describing the interaction between sorbate particles and atoms composing the solid, and z_i is the vertical distance between the center of the ith sorbate particle and the solid wall. Given these three types of interactions, the total potential energy of the N_s sorbate particles is written as

$$\Psi = \psi_{ss} + \psi_{sw}^{(1)} + \psi_{sw}^{(2)} + \psi_{sp}, \tag{8}$$

where $\psi_{sw}^{(1)}$ and $\psi_{sw}^{(2)}$ are used to indicate the potential energies associated with the presence of the upper and lower walls.

The state conditions of the sorbate particles are specified by a dimensionless temperature T and a dimensionless number density ρ_s, given by

$$T = \frac{k}{3N_s\epsilon_{ss}}\sum_{i}^{N_s} v_i^2 \tag{9}$$

$$\rho_s = \frac{N_s}{\varphi l^2(h-1)\sigma_p} \tag{10}$$

where v_i is the velocity of the ith sorbate particle, and k is Boltzmann's constant.

Calculations

At the outset, several variables need to be specified. These are the geometric parameters h, φ, σ_p, and l, the interaction parameters ϵ_{ss}, σ_{ss}, ϵ_{sp}, σ_{sp}, ϵ_{sw}, and σ_{sw}, the state conditions of sorbate particles T and ρ_s, and the simulation parameters such as the magnitude of the time step, number of simulation steps, and the cutoff distance of the potential r_c. For simplicity, we chose identical interaction parameters for sorbate-sorbate, sorbate-pillar, and sorbate-solid interactions. Therefore, in what follows we delete all subscripts and simply use ϵ and σ to represent the energy and size parameters. Of course, it is not difficult to use different energy and size parameters for the various pairs. The characteristic diameter of a pillar unit is chosen the same as the size parameter σ. Hereafter, all lengths are expressed in units of σ and all energies in units of ϵ. The separation distance h between the solid walls is varied as one parameter of our simulations. In pillared clays h is about 12–20 Å, and if we use $\sigma = 3.405$ Å, the value for argon (as we do in our simulations), we obtain $h = 4$–6 (in units of σ). We used periodic boundary conditions in the x-y direction, and thus the size of the cell representing the system is selected such that the number of sorbate particles it contains can statistically represent the desired density, and is considered reasonable from a computational point of view. We found this size to be typically around $l = 9$. The porosity φ was varied anywhere between 1 (a slit pore) and the percolation threshold φ_c of the system, the critical porosity below which no macroscopic diffusion is possible, to study the effect of porosity on the diffusivity. The temperature of the system was fixed at 1.2, and the density ρ_s of the sorbate particles was varied from 0 to 0.6 to study the density dependence of the diffusivity.

Although a few articles have discussed the pore-size distribution of pillared clays, calculated from adsorption isotherms and molecular probe measurement (Baksh et al., 1992; Yang and Baksh, 1991; Baksh and Yang, 1992), the spatial distribution of the pillars is not completely understood yet. Therefore, we studied two different spatial distributions of the pillars, namely, a random distribution and a uniform one. In the uniform distribution, the pillars are distributed on the site of a square lattice (see Figure 2). The lattice parameter should, in principle, be calculated from the specified porosity φ and the length of the unit cell l. However, since the number of pillars N_p can only be the square of an integer number, it is not practical to specify φ directly at the beginning of the simulations. What we did instead was find first the appropriate

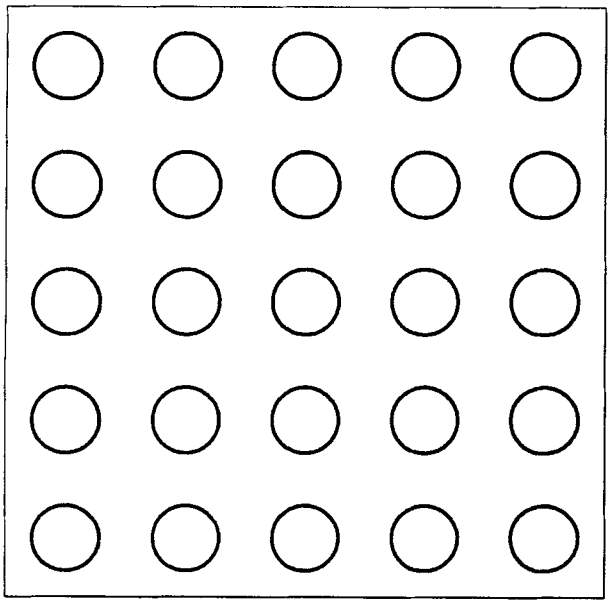

Figure 2. Uniform distribution of the pillars with porosity $\varphi = 0.8383$.

values of l and N_p that gave a porosity close enough to the one we wished to perform our simulations at, and then distribute the pillars with their coordinates given by

$$x_i^p = (0.5 + i)a, \tag{11}$$

$$y_i^p = (0.5 + i)a, \tag{12}$$

where $i = 1, 2, \ldots, \sqrt{N_p}$, and $a = 1/\sqrt{N_p}$ is the lattice parameter. Two types of random distribution of the pillars are used. In one of them the positions of the (centers of the) pillars are determined by the following equations

$$x_i^p = Rl \tag{13}$$

$$y_i^p = Rl \tag{14}$$

where R is a random number distributed uniformly in (0,1). This allows overlap of the pillar units, and in general results in a smaller excluded volume than for the uniform distribution of the pillars (the effective porosity is higher), especially at low porosities. Allowing for pillar overlap also makes it possible to simulate a system in which the overlapped pillars act effectively as irregularly shaped pillars with varying effective sizes. In the second type of random distribution of the pillars, no overlap is allowed between the pillars. By comparing the results for the uniform and random systems, we gain insight into the effect of the spatial distribution of the pillars on the effective diffusivity.

A standard fifth-order Gear predictor-corrector algorithm (Gear, 1971) was used to integrate Newton's equation of motion. The simulation begins with the construction of the porous system according to the specified configuration, followed by a random assignment of momenta and positions to the N_s sorbate particles, subject to the constraint of zero total momentum. The first several thousand time steps of the simulations were spent for system equilibration, in which the velocities of particles were scaled and adjusted periodically according to the specified temperature of the system. These adjustments were terminated once the difference between the simulated and the specified temperature was less than 0.005. Then the trajectories of the molecules were determined for a number of simulation steps (usually several tens of thousands). No temperature adjustments were made during that part of the simulations over which the desired statistics were collected.

In general, the magnitude of the time step and the number of simulation steps depend on the porosity of the system and the density of the sorbate particles. The magnitude of the time step is mainly dictated by the energy fluctuations during the simulations. In our simulations the typical time step used was 0.00462, equivalent to 0.01 ps if we set ϵ/k_b and σ equal to 119.8 K and 3.405 Å, respectively, the values for argon. With this time step, in most cases that we studied, the energy fluctuations in 10,000 steps varied at most 0.04% of the average value. As for the number of simulation steps, 10,000 time steps were generally sufficient to represent the ensemble averages for slit pores. For the pillared systems, however, longer simulation times were required for obtaining accurate statistics. In this case, the typical number of simulation steps we used was 40,000.

Once the trajectories were determined, the properties of interest such as the diffusivity and the solvation force were evaluated. For example, to evaluate the diffusivity, we may use either the Einstein equation

$$D = \frac{1}{6N_s} \lim_{t \to \infty} \left\langle \sum_{i=1}^{N_s} \frac{|\boldsymbol{r}_i(t + t_0) - \boldsymbol{r}_i(t_0)|^2}{t} \right\rangle, \tag{15}$$

or the Green-Kubo equation

$$D = \frac{1}{3} \int_0^\infty \left\langle \sum_{i=1}^{N_s} [\boldsymbol{v}_i(t + t_0)\boldsymbol{v}_i(t_0)] \right\rangle dt, \tag{16}$$

where $\langle \cdot \rangle$ indicates an average over all trajectories with a series of independently selected time origins t_0. Because of the small distance between the solid walls, the porous system is anisotropic and should be characterized by two effective diffusivities. Thus, if D_l and D_t denote the longitudinal diffusivity (in the direction parallel to the solid walls) and the transverse diffusivity (in the direction perpendicular to the solid walls), they are calculated by the following equations

$$D_t = \frac{1}{2N_s} \lim_{t \to \infty} \left\langle \sum_{i=1}^{N_s} \frac{[z_i(t + t_0) - z_i(t_0)]^2}{t} \right\rangle, \tag{17}$$

$$D_l = \frac{1}{4N_s} \lim_{t \to \infty} \times \left\langle \sum_{i=1}^{N_s} \frac{[x_i(t + t_0) - x_i(t_0)]^2 + [y_i(t + t_0) - y_i(t_0)]^2}{t} \right\rangle, \tag{18}$$

or by

$$D_t = \int_0^\infty \left\langle \sum_{i=1}^{N_s} [v_{zi}(t+t_0)v_{zi}(t_0)] \right\rangle dt, \tag{19}$$

$$D_l = \frac{1}{2}\int_0^\infty \left\langle \sum_{i=1}^{N_s} [v_{xi}(t+t_0)v_{xi}(t_0) + v_{yi}(t+t_0)v_{yi}(t_0)] \right\rangle dt. \tag{20}$$

Although both methods were used in this study, we report here the results that were obtained using the Einstein equation, because the results obtained with both methods are comparable for simulations of limited durations, and the Einstein equation approach is generally considered more reliable for describing the long time diffusive behavior of the molecules than the Green-Kubo equation (June et al., 1990). Because the distance between the walls is finite, D_t vanishes as $t \to \infty$. Thus, we refer to $D_l = D$ as the effective diffusivity of the molecules.

Two other properties, the solvation force and the density distribution function of the molecules, are also calculated from the trajectories. The solvation force f_s, defined as the force per unit wall area exerted by all sorbate particles, is calculated by the following equation:

$$f_s = \frac{1}{l^2}\left\langle \sum_{i=1}^{N_s} \left[\frac{\partial \psi_{sw}(z)}{\partial z} \right]_{z = h\sigma_p} \right\rangle, \tag{21}$$

where the averaging is over the duration of the simulation. The term f_s is calculated for only one wall, since in the absence of gravity (which we ignore) the system is symmetric, that is, the force experienced by the two walls must be the same. The density distribution function $\chi(z)$ is evaluated from the following equation

$$\chi(z) = \frac{1}{l^2}\left\langle \frac{\partial N(z)}{\partial z} \right\rangle, \tag{22}$$

where $N(z)$ is the number of sorbate particles distributed between 0 and z.

A random distribution of the pillars necessitates calculation of the average values for all quantities of interest, where the averaging must be taken over several realizations of the random system at a fixed porosity. This is done by first calculating the quantities of interest for each realization, and then averaging the results among the realizations. The number of realizations depends on the porosity of the system, and the desired accuracy of the results. If, for example, a 10% variation among all realizations is acceptable, then a few realizations may suffice. However, if one needs estimates of the quantities of interest with a much higher accuracy, then a large number of realizations may be needed. Moreover, as the porosity of the system decreases, sample-to-sample fluctuations also increase, and one needs an increasingly larger number of realizations of the random system to obtain reliable statistics.

Table 1. Solvation Force as a Function of the Porosity of the System and the Molecular Density*

	Density			
Porosity	0.15	0.30	0.45	0.60
1.0000	−0.18	−0.38	−0.14	1.07
0.9741	−0.17	−0.32	−0.03	1.10
		(−0.27)	(−0.05)	(1.14)
0.9418	−0.15	−0.25	0.10	1.26
		(−0.23)	(0.06)	(1.13)
0.8965	−0.14	−0.12	0.51	1.25
		(−0.12)	(0.27)	(1.37)
0.8384	−0.02 (0.03)*	0.15		

*Numbers in parentheses refer to those for a random configuration of the pillars, while the rest are for a uniform pillar configuration.

Results

First we carried out some simulations for slit pores (pores without pillars). The separation distance between the solid walls and corresponding sorbate density were chosen to be the same as those used by Snook and van Megan (1980) in their GCEMC study of slit pores. Our results for the solvation force and the density distribution were in good agreement with theirs. The diffusivity D was also in good agreement with the MD results reported by Magda et al. (1985) for the same system, thus confirming the validity of our simulations.

Figure 2 shows a uniform spatial distribution of the pillars corresponding to the lowest porosity used in our study, which, from a computational viewpoint, was also the most difficult pore space configuration used in this study. In this system, the distance between the nearest-neighbor pillars is 1.8.

Solvation force and the density distribution

In Table 1 the solvation force f_s is shown as a function of the sorbate density and porosity for a uniform distribution of the pillars and a random distribution in which the pillars are allowed to overlap. The results for the two distributions do not exhibit a significant difference. In both cases f_s increases monotonically with decreasing porosity, which may be explained by considering the structure of the pillared clays. As the porosity of the system decreases, the motion of the sorbate particles is increasingly confined to the transverse direction, that is, within the vertical pores formed by the pillars. As a result, the solid walls experience more repulsion, and thus f_s increases with decreasing φ. On the other hand, f_s increases with increasing molecular density, since higher molecular densities also result in larger repulsive forces.

As discussed earlier, a random distribution of the pillars implies that one has to average the results over several realizations of the system. In Table 1 we compared the results for a uniform pillar distribution and a random one in which the pillars are allowed to overlap, for several particle densities. We now fix the density and compare the results for the uniform system with a random one in which the pillars are not allowed to overlap. To obtain a better understanding of how the quantities of interest vary among different realizations of the random system, we calculated f_s and the diffusivity D (the results of which are discussed below) for several differ-

ent realizations of the random system. We fixed the sorbate density at $\rho_s = 0.3$ and the separation distance between the walls at $h = 4$ for all realizations. To obtain a quantitative measure of the deviations of the random system from the uniform one, we define a quantity A

$$A = \sum_{r}^{l/2} [g^{(r)}(r) - g^{(u)}(r)]^2. \tag{23}$$

Here $g(r)$ is the two-dimensional radial distribution function of the pillars, and is defined by

$$g(r) = \frac{\langle N(r \pm \delta r/2) \rangle}{2\pi r \delta r \rho}, \tag{24}$$

were $N(r \pm \delta r/2)$ is the number of pillars in a spherical shell of thickness δr located at a distance r from the center of a pillar, and $\langle \cdot \rangle$ denotes an average over all pillars inside the cell. Superscripts r and u denote the distribution function for the random and uniform systems, respectively. Calculations were carried out for two porosities at 0.941 and 0.896. The $\varphi = 0.941$ system corresponds to 9 pillars inside a 9×9 cell. Thus, the typical distance between two pillars is $2\sigma \simeq 7$ Å, which is in the range of experimental values for the distance between the pillars, which is about 5–10 Å (Pinnavaia, 1983). The $\varphi = 0.896$ system corresponds to 16 pillars inside a 9×9 cell.

Figure 3 compares the solvation forces among seven realizations of the random system with no pillar overlap at porosity $\varphi = 0.941$, with that of a uniform system (for which $A = 0$) at the same porosity. As can be seen, except for one realization, there is at most 10% variation among various realizations. Moreover, the average solvation force between all realizations is only a few percent different from that of the uniform system. Figure 4 makes the same comparison, but at porosity $\varphi = 0.896$. In this case we compare four realizations

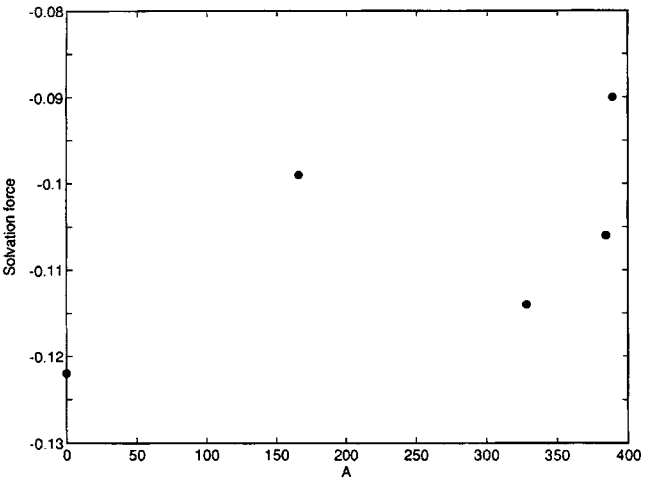

Figure 4. Same as in Figure 3, but with porosity 0.896.

of the random system with the uniform one. As in the case of the higher porosity system (Figure 3), there is about 15–20% variation between the three realizations. But, the difference between the average of the realizations and the uniform system is now somewhat larger than that at $\varphi = 0.941$.

Figure 5 presents the variations of the solvation force f_s with h, the separation distance between the walls, with a uniform distribution of the pillars, $\rho_s = 0.3$ and $\varphi = 0.941$. As h increases, f_s also increases, practically linearly with it. Figure 6 shows the porosity dependence of f_s for a random system without pillar overlap, and compares it with that of the uniform system. The separation distance is $h = 4$. The results for the random system represent the average of five realizations. At high porosities the relative difference between the two systems is small, but at low porosities the difference becomes significant.

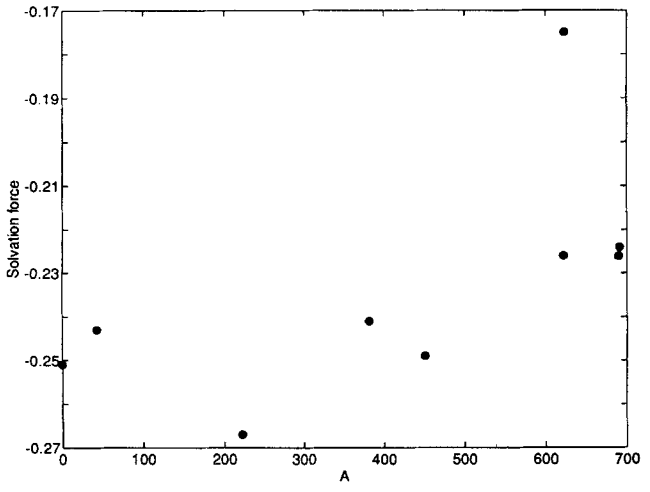

Figure 3. Solvation force for seven different realizations of a system vs. random distribution of the pillars with no overlap, with a uniform system (at $A = 0$) with the same porosity 0.941.

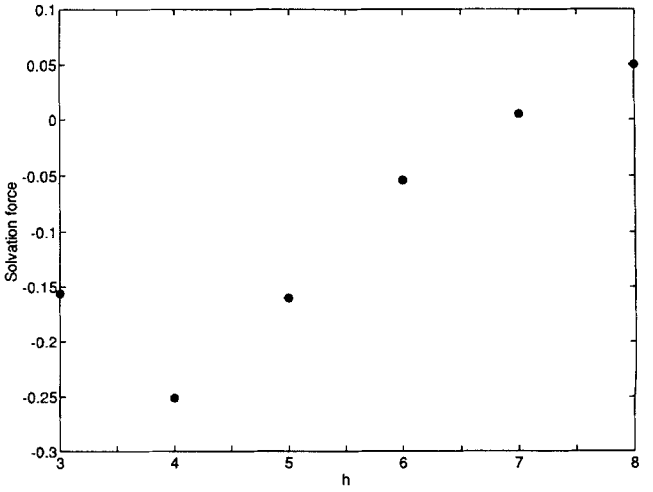

Figure 5. Dependence of the solvation force on the separation distance h between the solid walls.

The distribution of the pillars is uniform, the porosity is 0.941, and particle density is 0.3.

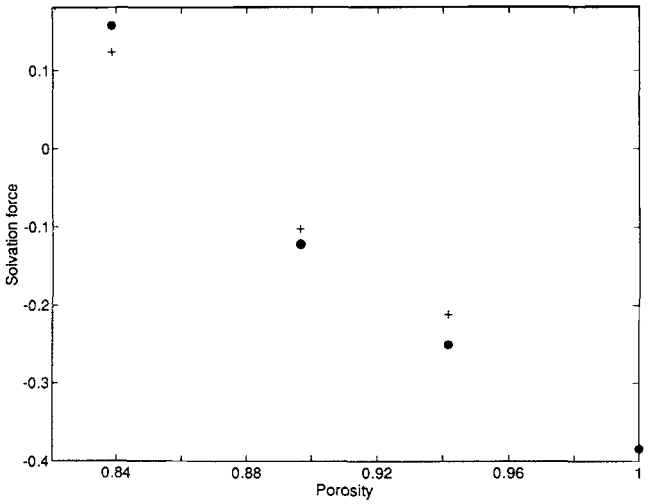

Figure 6. Comparison of porosity dependence of the solvation force for a random system without pillar overlap (+) with that of a uniform system (circles).

Particle density is $\rho_s = 0.3$ and the separation distance is $h = 4$.

Figure 7 represents the molecular density distribution for different porosities, a sorbate density $\rho_s = 0.45$, a uniform distribution of the pillars, and $h = 4$. This figure can also help us understand the porosity dependence of the solvation force shown in Table 1, if we note that f_s may also be evaluated from the molecular density distribution $\chi(z)$ through the following integral

$$f_s = -\int_0^h \frac{\partial \psi_{sw}(z)}{\partial z} \chi(z)\, dz. \tag{25}$$

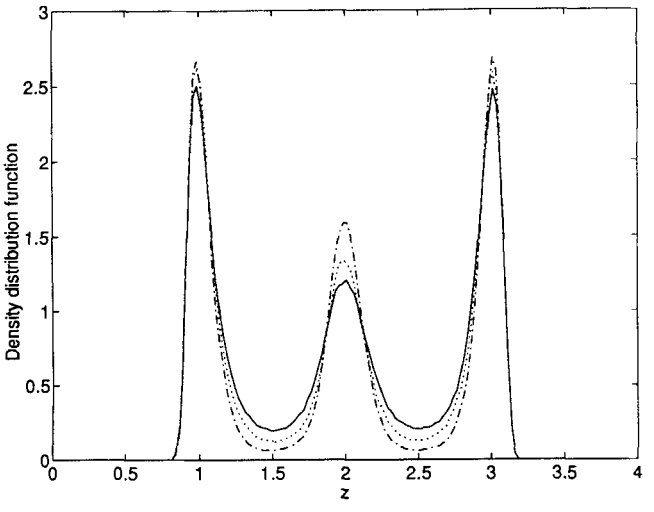

Figure 7. Molecular density distribution function as a function of the porosity φ for a uniform distribution of the pillars at sorbate density $\rho_s = 0.45$.

The solid curve is for $\varphi = 1.0$, the dotted curve for $\varphi = 0.974$, and the dashed-dotted curve for $\varphi = 0.896$.

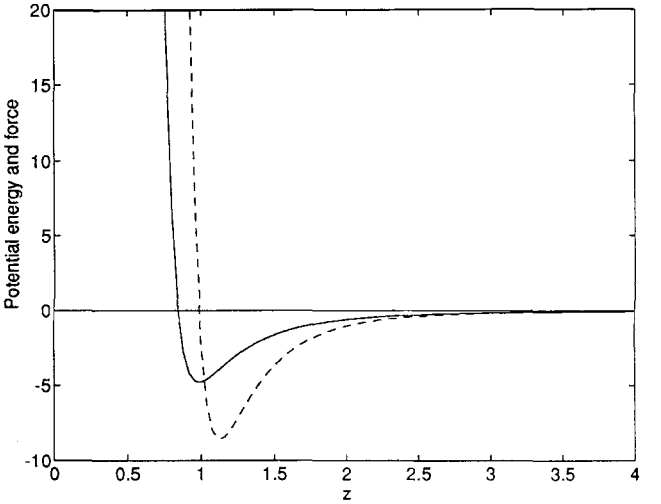

Figure 8. Potential energy (——) and force (---) between a solid wall and a sorbate particle as a function of the separation distance z.

The interaction between a sorbate particle and the solid walls changes from repulsive to attractive forces once the separation between the two is greater than 0.987 (see Figure 8). As Figure 7 indicates, the number of peaks remains the same as the porosity decreases from 1.0 to 0.8965, with one peak centering at the middle between two solid walls and the other two locating symmetrically at a distance of about 1.0 from each wall. The shape of the density distribution is, however, distorted slightly as the porosity decreases (the number of pillars increases). The net effect is smaller attractive interaction forces between the molecules and the walls due to competition from the pillars, which agrees with the results presented in Table 1. The same distortion of the density distri-

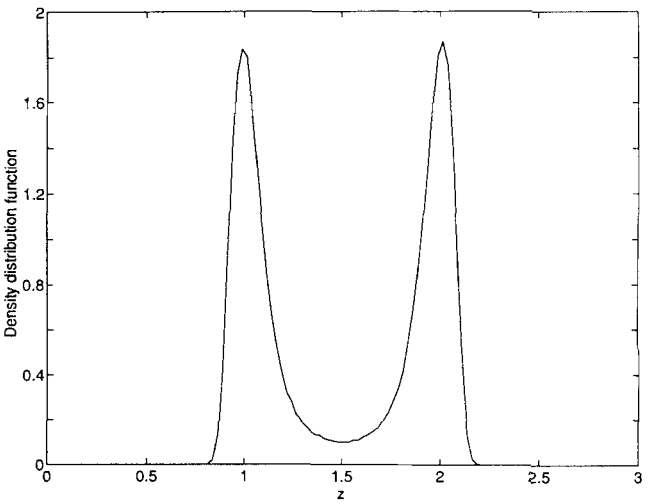

Figure 9. Molecular density distribution function as a function of the distance z from the center of the lower wall.

The distance between the walls is $h = 3$, the porosity is 0.941, and the pillar distribution is uniform.

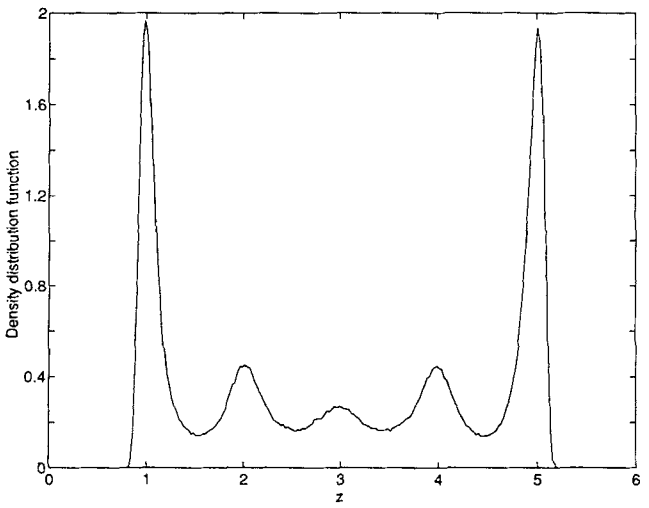

Figure 10. Same as in Figure 8, but with $h = 6$.

bution was also observed for a random distribution of the pillars.

To study how the density distribution function varies with h, a series of simulations was carried out with a uniform distribution of the pillars, a porosity $\varphi = 0.941$, and sorbate density $\rho_s = 0.3$. Figures 9–11 show the results for $h = 3$, 6, and 8. As can be seen, the number of peaks in the distribution is $[h - 1]$. The heights of the two peaks near the solid walls increase with h, as do those of the smaller peaks in between.

In Figure 12 the density distribution functions for a uniform distribution of the pillars and several sorbate densities at a fixed porosity $\varphi = 0.941$ and $h = 4$ are shown. Compared with Figure 9, the shape of the distribution changes as the sorbate density ρ_s varies. As ρ_s decreases from 0.6 to 0.3, the distribution function gradually becomes flatter, a trend similar to the variation of the radial distribution function with density in bulk fluids. The central peak almost disappears as ρ_s falls to 0.15, which explains the increase in the solvation force (less attractive force), shown in Table 1, as the density changes from 0.3 to 0.15.

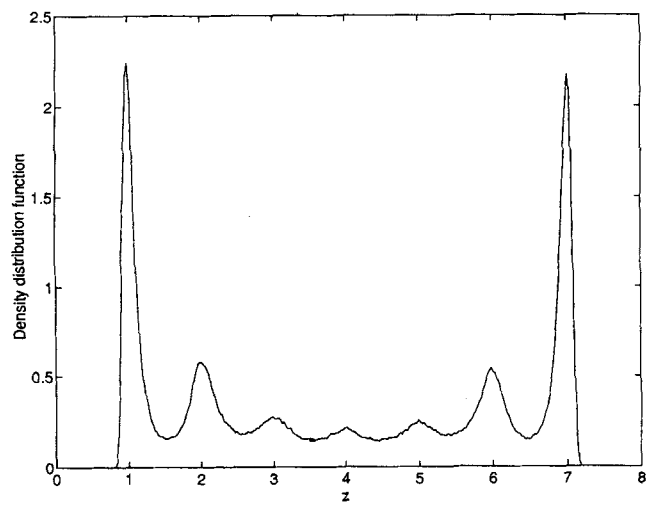

Figure 11. Same as in Figure 8, but with $h = 8$.

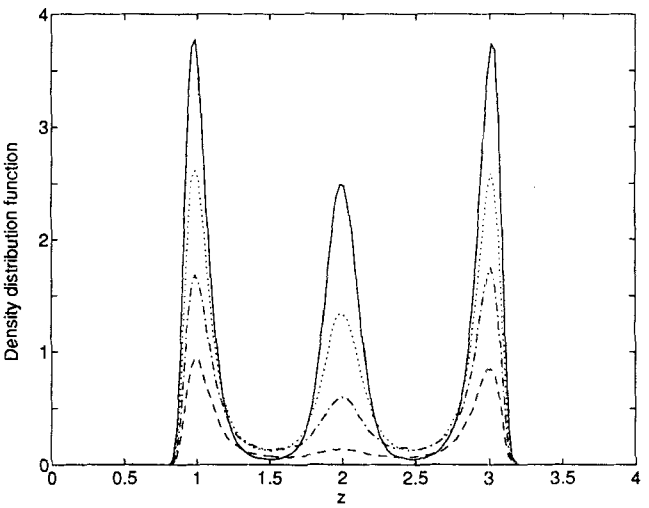

Figure 12. Molecular density distribution function as a function of the molecular density ρ_s for a uniform distribution of the pillars with porosity $\varphi = 0.941$, as a function of the distance z from the center of the lower wall.

Solid curve is for $\rho_s = 0.6$, dotted curve for $\rho_s = 0.45$, dashed-dotted curve for $\rho_s = 0.3$, and dashed curve for $\rho_s = 0.15$.

Diffusivity

Figure 13 presents the time dependence of the longitudinal and transverse mean square displacements, corresponding to the uniform distribution of the pillars shown in Figure 2, while Figure 14 shows the corresponding longitudinal diffusivity. As Figure 13 indicates, the mean square displacements vary linearly with time and their slopes reach a constant value after about 50 ps. The resulting transverse diffusivity is, however,

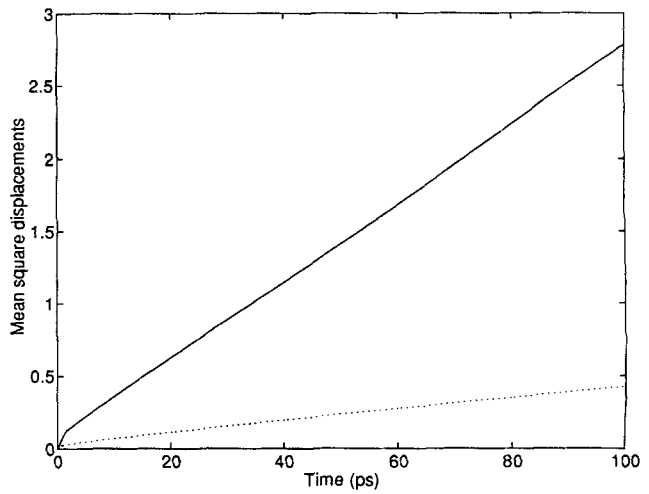

Figure 13. Longitudinal (——) and transverse (---) mean square displacements, corresponding to the pillar distribution of Figure 2 and $\rho_s = 0.3$.

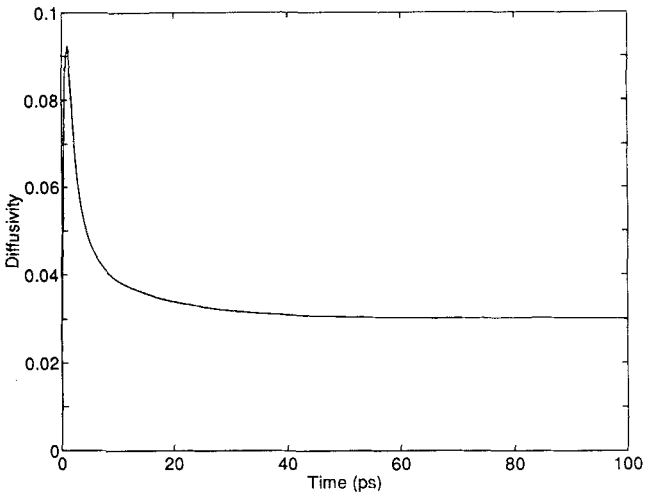

Figure 14. Longitudinal diffusivity calculated from Figure 13.

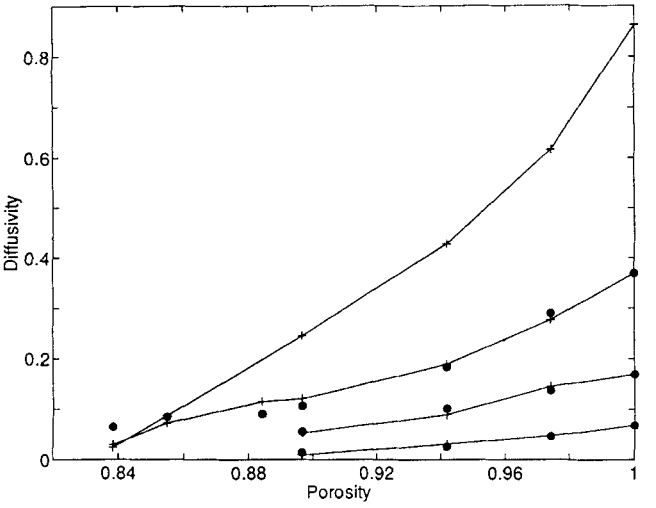

Figure 15. Porosity dependence of the diffusivity for random and uniform distribution of the pillars for several sorbate densities.

The points marked by + and • are for the uniform and random distribution of the pillars with overlap, respectively. The results are, from top to bottom, for $\rho_s = 0$, 0.3, 0.45, and 0.6, respectively.

very small. The time t_d required for reaching such a diffusive behavior is shorter for pillar configurations with higher porosities. This is in agreement with percolation theory (Stauffer and Aharony, 1992; Sahimi, 1994) that predicts that as the percolation threshold φ_c of the system is approached, t_d diverges according to the following scaling law

$$t_d \sim (\varphi - \varphi_c)^{-\theta}, \tag{26}$$

where θ is a universal exponent (independent of the microscopic details of the system), and $\theta \simeq 3.82$ and 3.34 for two- and three-dimensional systems, respectively.

Figure 15 compares the effective diffusivity D at different porosities and sorbate densities for a uniform distribution of the pillars and a random distribution in which the pillars are allowed to overlap. The separation distance between the solid walls is fixed at $h = 4$. As this figure indicates, the diffusivity increases with increasing porosity, but decreases as the density increases. The reason is not very difficult to understand. Both the decrease in the porosity and the increase in sorbate density result in an increased frequency of sorbate-pillar and sorbate-sorbate collisions, and thus decrease the mobility of the sorbate particles. As can be seen in Figure 15, at high porosities up to $\varphi = 0.941$ the diffusivities for random and uniform distribution of the pillars at the same conditions do not differ from each other significantly. As the porosity further decreases, however, the effect of the spatial distribution of the pillars on the diffusivity begins to manifest itself. At porosity $\varphi = 0.8383$ (corresponding to 25 pillars inside a 9×9 unit cell), the diffusivity for a random distribution of the pillars is twice as larger as that of the uniform distribution of the pillars, while the relative differences for the other four larger porosities are at most $\pm 20\%$. This may be attributed mainly to the effect of clustering of the pillars when they are distributed randomly in a system with a low porosity. For example, Figure 16 presents the configuration of the randomly distributed pillars within the unit cell at porosity $\varphi = 0.8383$, in which the pillars are allowed to overlap. As can be seen, considerable overlap of the pillars occurs, resulting in a smaller excluded volume and creating some interconnected pores with dimensions larger than those of the corresponding pores generated with a uniform distribution of the pillars (see Figure 2 for comparison), which consequently increase the diffusivity of the sorbate particles. This should be compared with Figure 17 in which the pillars are randomly distributed, but are not allowed to overlap.

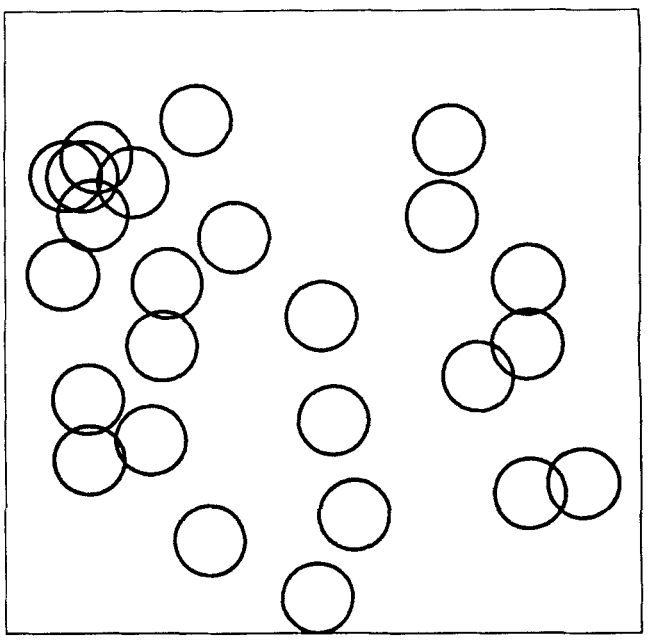

Figure 16. Clustering of the pillars with a random distribution and porosity 0.8383.

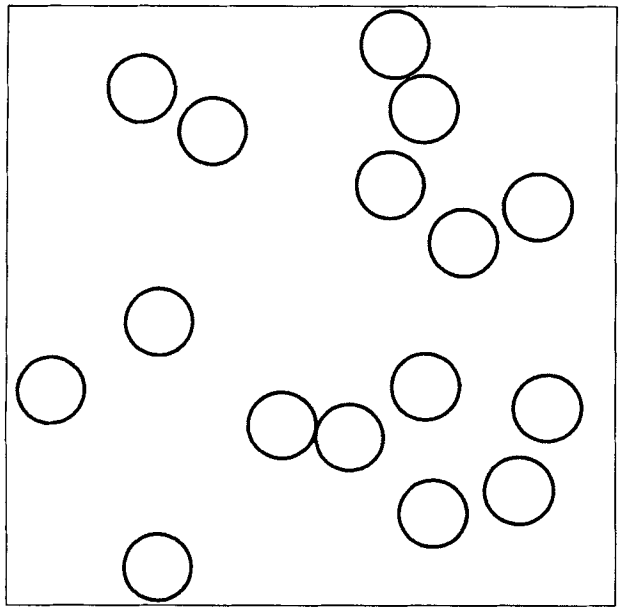

Figure 17. Typical random configuration of the pillars in which they are not allowed to overlap.

Figure 18 compares the diffusivities of seven different realizations of a random system with no pillar overlap with that of a uniform system, for $\varphi = 0.941$, $\rho_s = 0.3$, and $h = 4$, which generate the same pillar configuration as that of Figure 3. As can be seen, the largest diffusivity is only 10% larger than the smallest diffusivity. Moreover, the average diffusivity among all seven realizations differs from that of the uniform system by only about 3%. Figure 19 makes the same comparison, but for $\varphi = 0.896$. All other parameters of the system are the same as those for the system of Figure 18. In this case there is a larger difference between different realizations, and the difference between the average of the realizations and that of the uniform system is also larger than that of the $\varphi = 0.941$. Figure 20 compares the porosity dependence of the diffusivity of a random system without pillar overlap with that of a uniform system. The results for the random system represent an average over five different realizations of the system, and the separation distance is $h = 4$. As in the case of the solvation force, while at high porosities the difference between the two diffusivities is small, at low porosities the relative difference is significant. Moreover, only at low porosities the difference between the diffusivities of a random system with and without pillar overlap is significant.

Based on the comparison between the uniform and random systems, we may draw two conclusions: (1) as the porosity of the system decreases, one needs a larger number of realizations of the random system in order to obtain representative statistics; and (2) while at high porosities uniform and random distributions of the pillars may yield comparable estimates of various quantities of interest, the difference be-

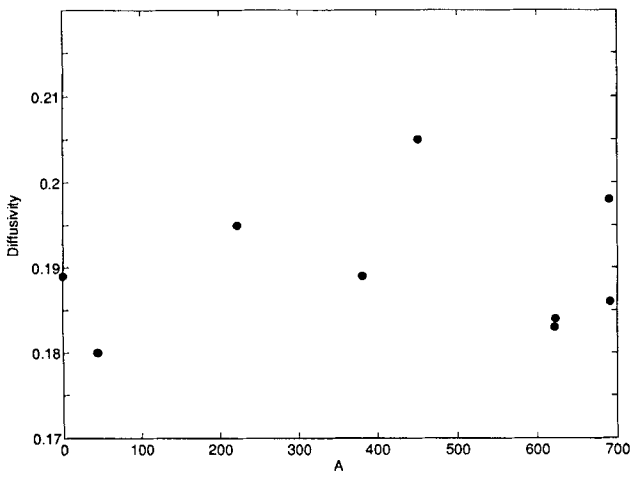

Figure 18. Diffusivity for seven different realizations of a random system with no pillar overlap, vs. that of a uniform system (at $A = 0$) with the same porosity 0.941.

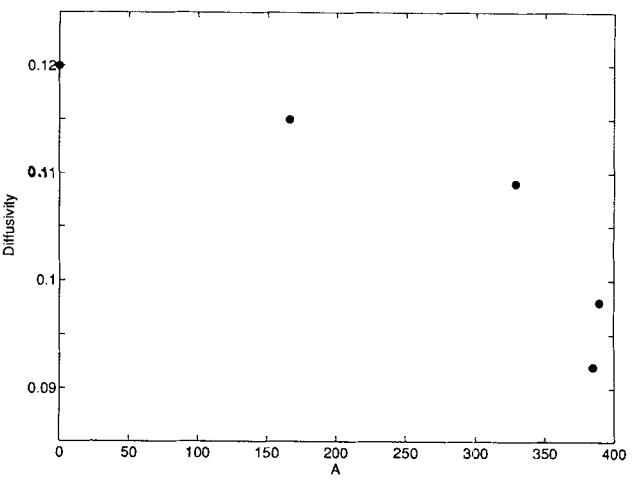

Figure 19. Same as in Figure 18, but for porosity 0.896.

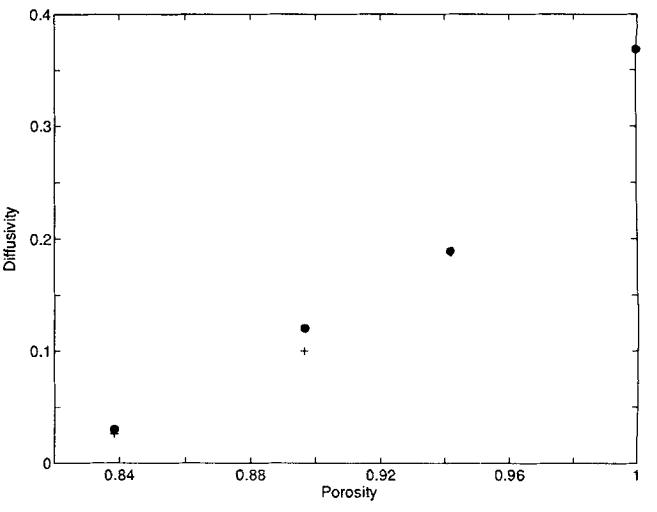

Figure 20. Porosity dependence of the diffusivity of a uniform system (•) with that of a random system (+) without pillar overlap.

Particle density is $\rho_s = 0.3$ and the separation distance is $h = 4$.

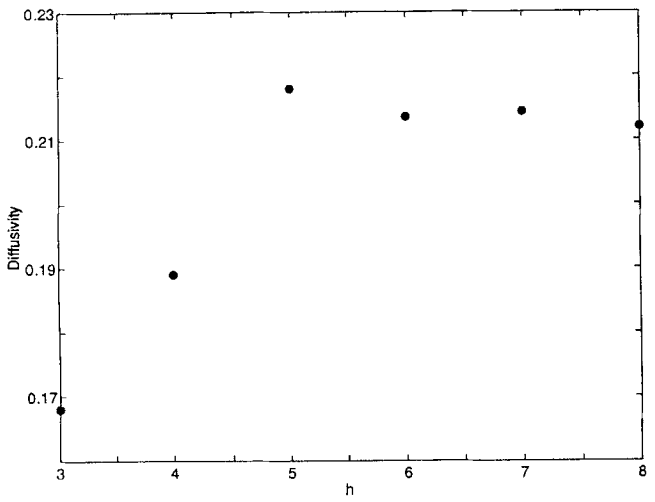

Figure 21. Dependence of the diffusivity on the separation distance h between the solid walls.

The pillar distribution is uniform, the porosity is 0.941, and particle density is 0.3.

tween the two systems increases as the porosity of the system decreases, and may become relatively large at porosities near the percolation threshold. However, if, for example, a 15–20% difference between the properties of the two systems is acceptable, then the uniform system may still yield reasonable estimates of the quantities of interest for a random system.

Figure 21 presents the dependence of D on the separation distance h between the solid walls in a system with a uniform distribution of the pillars, $\rho_s = 0.3$, and $\varphi = 0.941$. As expected, for small values of h the diffusivity increases with h, but for $h > 5$ it attains an essentially constant value, implying that for $h > 5$ the system is effectively three-dimensional, which is why D becomes independent of h. Note that with $\sigma = 3.405$ Å, which we used in our simulations, $h = 6$ is equivalent to $h \simeq 20$ Å, which is about the upper limit of the distance between the silicate layers in most pillared clays.

Diffusion near the percolation threshold

An important characteristic property of porous systems is their percolation threshold φ_c (Stauffer and Aharony, 1992; Sahimi, 1994). Of particular interest is the behavior of the diffusivity near φ_c. For our system, such low porosities may be generated by a dense distribution of the pillars. In practice, low porosities can also be generated if large molecules, such as normal alkanes, are adsorbed on the pillars, hence plugging the pores, which is in fact often the case. To study this, we performed a series of simulations with a uniform distribution of the pillars at zero particle density, which is realized simply by removing the interactions between the sorbate particles, so that they do not feel the presence of each other. Percolation theory predicts that as the critical porosity φ_c is approached, the effective diffusivity vanishes according to the following power law

$$D \sim (\varphi - \varphi_c)^n, \qquad (27)$$

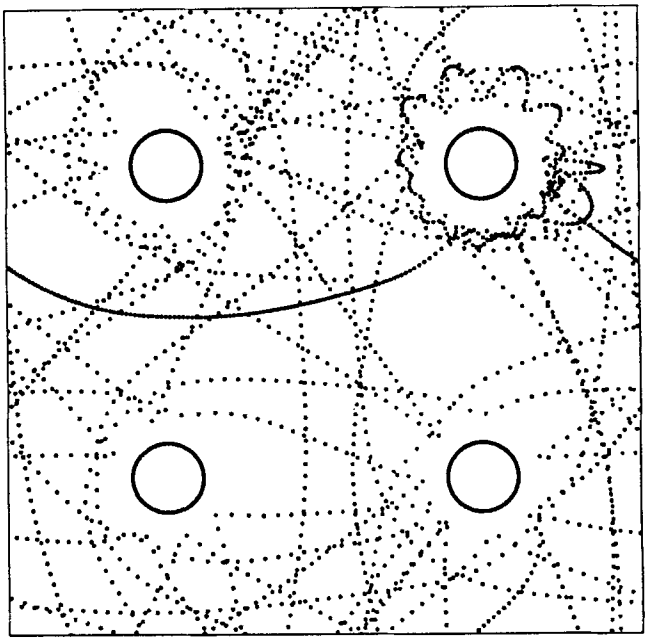

Figure 22. Trajectory of a particle in a system with porosity $\varphi = 0.9741$ and a uniform distribution of the pillars at infinite molecular dilution.

where $n \simeq 1.3$ and 2 for two- and three-dimensional systems, respectively. The disappearance of D can be illustrated graphically by observing the trajectories of a single randomly selected sorbate particle in two systems with porosities $\varphi \simeq 0.9741$ and 0.8383. As shown in Figures 22 and 23, both sys-

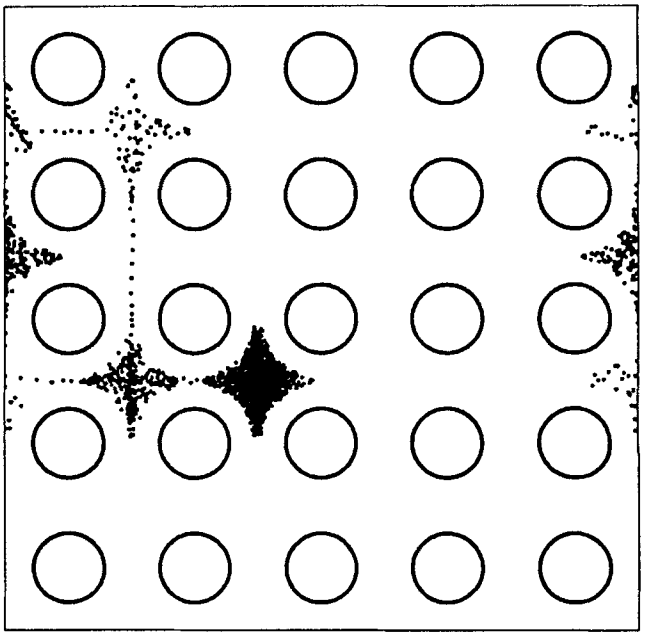

Figure 23. Trajectory of a particle in a system with porosity 0.838, and a uniform distribution of the pillars at infinite molecular dilution.

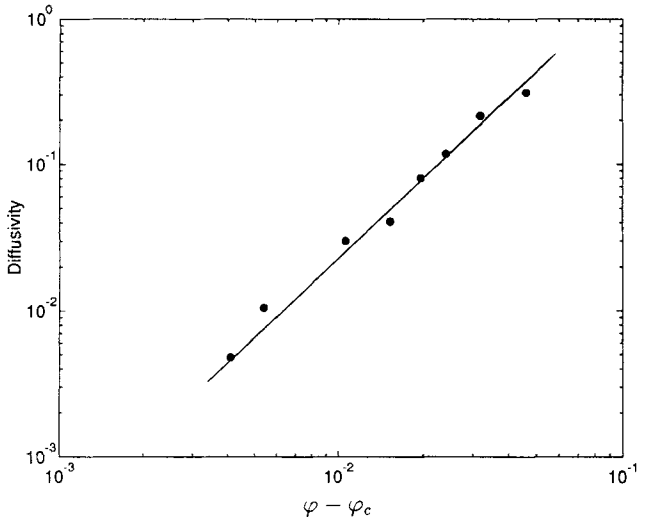

Figure 24. Power law behavior of the diffusivity near the percolation threshold.

The straight line is the best fit of the data.

tems correspond to a uniform distribution of the pillars at zero molecular density. At the higher porosity (Figure 23) the sorbate particle can move almost freely in the longitudinal directions, since there are very few pillars inside the cells. As the porosity decreases, molecular motion along the longitudinal directions becomes more difficult. Eventually, the sorbate particle is mostly entrapped at some low energy zones as the porosity approaches its threshold, as indicated by Figure 23.

To obtain an estimate of φ_c and n, the results at low φ are plotted logarithmically in Figure 24, and from a linear regression we obtain $\varphi_c \simeq 0.8250$ and $n \simeq 1.7$. For a system of hard-sphere pillars and sorbate particles diffusion ceases when the distance between the pillars is equal to $\sqrt{3}\sigma$. Therefore, the critical porosity is given by (see Eq. 1) $\varphi_c = 1 - \pi/18 \simeq 0.8255$, in perfect agreement with our estimate, which is also indicative of the accuracy of our simulations. On the other hand, the fact that our value of n is between those of two- and three-dimensional systems may mean that, to the extent that our model is a realistic representation of pillared clays, such systems have an effective dimensionality between two and three. Percolation theory also tells us that n is independent of the microscopic details of the system. We thus expect n to be the same for uniform and random distribution of the pillars.

Summary

In this article, a model of pillared clays was developed and extensive molecular dynamics simulation of diffusion in such systems was carried out. Various properties of interest, including the solvation force, the molecular density distribution function, and the effective diffusivity and its critical behavior near the percolation threshold were studied for three different spatial distributions of the pillars, at molecular densities ranging from 0 to 0.6 and porosities ranging from 1.0 to 0.8270. The solvation force was found to be monotonically increasing with decreasing porosity, and its nature changed from a repulsive to an attractive force when the sorbate density was varied from 0.6 to 0.3. The molecular density distribution functions were found to be distorted as the porosity and sorbate density were varied, in a manner consistent with the porosity and density dependence of the solvation force. The diffusivities for the three distinct pillar distributions did not differ significantly from each other at high porosities. But the difference became significant at low porosities, that is, at porosities not far from the percolation threshold of the system. This may have significance for practical applications, as adsorption of large molecules on the pillars, which often occurs in practical use of pillared clays, plugs the pores and gives rise to low porosity clays. Near the percolation threshold, the effective diffusivity was found to follow a power law with an exponent $n \simeq 1.7$. To the extent that our model is a realistic representation of pillared clays, this result implies that the system has an effective dimensionality between two and three.

Work is currently in progress to study the temperature dependence of the various properties of the system. The effect of preferential adsorption on the wall or the pillar on the diffusivities is also under study, as is that of the molecular shapes. The results will be reported in a future article.

Acknowledgments

This work was supported by the National Science Foundation under grant CTS-9122529. The work of M. S. was also supported in part by the Department of Energy. M. S. is grateful to Hans Herrmann and the HLRZ-KFA Supercomputer Center in Jülich, Germany, where part of the computations were carried out, for warm hospitality.

Literature Cited

Baksh, M. S. A., E. S. Kikkinides, and R. T. Yang, "Characterization by Physisorption of a New Class of Microporous Adsorbents: Pillared Clays," *Ind. Eng. Chem. Res.*, **31**, 2181 (1992).

Baksh, M. S. A., and R. T. Yang, "Unique Adsorption Properties and Potential Energy Profiles of Microporous Pillared Clays," *AIChE J.*, **38**, 1357 (1992).

Barrer, R. M., and D. M. MacLeod, "Activation of Montmorillonite by Ion Exchange and Sorption Complexes of Tetra-alkyle Ammonium Montmorillonites," *Trans. Farad. Soc.*, **51**, 1290 (1955).

Brindley, G. W., and R. E. Sempels, "Preparation and Properties of Some Hydroxy-Aluminum Beidellites," *Clays Clay Miner.*, **12**, 229 (1977).

Cracknell, R., C. A. Koh, S. M. Thompson, and K. E. Gubbins, "Molecular Simulation of Adsorption of Simple Gases in Aluminophosphates and Pillared Clays," *Mat. Res. Soc. Symp. Proc.*, **290**, 135 (1993).

Deen, W. M., "Hindered Transport of Large Molecules in Liquid-Filled Pores," *AIChE J.*, **33**, 1409 (1987).

Figueras, F., "Pillared Clays as Catalysts," *Cat. Rev.-Sci. Eng.*, **30**, 457 (1988).

Gear, C. W., *Numerical Initial Value Problems in Ordinary Differential Equations*, Prentice-Hall, Englewood Cliffs, NJ (1971).

Grim, R. E., *Clay Mineralogy*, McGraw-Hill, New York (1986).

June, R. L., A. T. Bell, and D. N. Theodorou, "Molecular Dynamics Study of Methane and Xenon in Silicalite," *J. Phys. Chem.*, **94**, 1508 (1990).

Kerr, G. T., "Synthetic Zeolites," *Sci. Amer.*, **261**, 100 (1989).

Lahav, H., V. Shani, and J. Shabtai, "Cross-Linked Smectites: I. Synthesis and Properties of Hydroxy-Aluminum Montmorillonite," *Clays Clay Miner.*, **26**, 107 (1978).

Laszlo, P., "Chemical Reaction on Clays," *Science*, **235**, 1473 (1987).

Lee, W. Y., R. H. Raythatha, and B. J. Tatarchuk, "Pillared-Clay Catalysts Containing Mixed-Metal Complexes. I. Preparation and Characterization," *J. Cat.*, **115**, 159 (1989).

Magda, J. J., M. V. Tirrell, and H. T. Davis, "Molecular Dynamics of Narrow, Liquid-Filled Pores," *J. Chem. Phys.*, **83**, 1888 (1985).
Occelli, M. L., R. A. Innes, F. S. S. Hwu, and J. W. Hightower, "Sorption and Catalysis on Sodium-Montmorillonite Interlayered with Aluminum Oxide Clusters," *Appl. Cat.*, **14**, 69 (1985).
Pinnavaia, T. J., "Intercalated Clay Catalysts," *Science*, **220**, 365 (1983).
Sahimi, M., "Diffusion, Adsorption, and Reaction in Pillared Clays. I. Rod-Like Molecules in a Regular Pore Space," *J. Chem. Phys.*, **92**, 5107 (1990).
Sahimi, M., "Transport of Macromolecules in Porous Media," *J. Chem. Phys.*, **96**, 4718 (1992).
Sahimi, M., *Applications of Percolation Theory*, Taylor & Francis, London (1994).
Sahimi, M., G. R. Gavalas, and T. T. Tsotsis, "Statistical and Continuum Models of Fluid-Solid Reactions in Porous Media," *Chem. Eng. Sci.*, **45**, 1443 (1990).
Snook, I. K., and W. van Megan, "Solvation Forces in Simple Dense Fluids: I," *J. Chem. Phys.*, **72**, 2907 (1980).
Stauffer, D., and A. Aharony, *Introduction to Percolation Theory*, 2nd ed., Taylor and Francis, London (1992).
Steele, W. A., "The Physical Interaction of Gases With Crystalline Solids," *Surf. Sci.*, **36**, 317 (1973).
Vaughan, D. E. W., and R. J. Lussier, *Proc. Int. Conf. on Zeolites*, Naples (1980).
van Damme, H., and J. J. Fripiat, "A Fractal Analysis of Adsorption Process by Pillared Swelling Clays," *J. Chem. Phys.*, **82**, 2785 (1985).
Yang, R. T., and M. S. A. Baksh, "Pillared Clays as a New Class of Sorbents for Gas Separation," *AIChE J.*, **37**, 679 (1991).

Manuscript received Dec. 3, 1993, and revision received Apr. 22, 1994.